

**GLOBAL STUDY OF THE MARTIAN SURFACE HYDRATION: NEW MEX/OMEGA DATA.** D. Jouglet<sup>1</sup>, F. Poulet<sup>1</sup>, Y. Langevin<sup>1</sup>, J.P. Bibring<sup>1</sup>, B. Gondet<sup>1</sup>. <sup>1</sup>IAS, Université Paris-Sud, 91495 Orsay Cedex, France, denis.jouglet@ias.fr.

**Introduction:** On Mars, surface hydration is one of the four water reservoirs detected by probes, with ice at the poles [1], vapor and clouds in the atmosphere [2] and ice in the sub-surface [3]. Hydration is known to be due to adsorbed water on the surface of minerals or inside specific sites of their structure, bound water to the lattice of minerals, or chemical metal-OH bonds. [4] Stretching and bending vibrations of the water molecule in hydration phase are responsible for a broad absorption band around 3  $\mu\text{m}$  in the surface reflectance spectra. The visible/near infrared OMEGA imaging spectrometer aboard the Mars Express probe gives the first opportunity to study globally and in detail the 3  $\mu\text{m}$  hydration band on Mars. Previous studies [4,5,6] focused on a part of the OMEGA dataset covering ~30% of the Martian surface. The coverage could not be larger because only orbits at nominal calibration levels were included in the study. This abstract presents the methods developed to derive new transfer functions for non nominal calibration data, so as to reach ~60% of the surface coverage for the hydration calculation. This abstract also presents an improvement of the water ice spectra rejection as an additional mean to increase the surface coverage. The first results associated to these new data are finally presented.

**Data processing and hydration assessment:** The OMEGA observations are released as the light flux (in Digital Numbers) received from Mars by the detector in the [0.3 – 5.1  $\mu\text{m}$ ] wavelength range. This raw data are calibrated to radiance emitted by the surface through the division by the OMEGA transfer function. Each spectrum is then corrected from atmospheric absorptions. The surface-diffused part and the thermal part of the spectrum are differentiated thanks to an estimation of the surface temperature through the radiance value at 5  $\mu\text{m}$ . The surface-diffused part of the spectrum, assumed to be lambertian, is then divided by the solar spectrum to get the albedo spectrum of the observed pixel [4,5]

Hydration is quantitatively estimated from albedo spectra thanks to the integration of the band depth (IBD) from 2.9 to 3.7  $\mu\text{m}$  between the albedo band and a linear continuum. An estimation of the water content (WC) is also performed, based on comparing the albedo ratio at 3  $\mu\text{m}$  over at 3.7  $\mu\text{m}$  with laboratory measurements [7] (albedo spectra measures of Martian-like samples at several hydration rates from 2 to 8 wt.%).

**Recalibration of non nominal data:** As exposed in [4,5] only a part of the OMEGA dataset could be studied for the hydration study because of the variations of the calibration state of the instrument. The calibration state is measured at the beginning of each orbit through the response of the instrument to an included lamp at several intensity levels. The instrument transfer function used to derive radiance from raw data is only available for the nominal behavior of the instrument.

*Variations of the calibration state.* In the near-infrared the OMEGA instrument is composed of two channels. Unlike the [1.0-2.5  $\mu\text{m}$ ] channel (named C) on which are based most of the OMEGA publications, the [2.5-5.1  $\mu\text{m}$ ] channel (named L) presents strong calibration variations during the mission. The level of these variations with the orbit number is plotted in Fig. 1. Data are considered as nominal when their calibration level is close to 1500 DN. This is the case for orbits 40 to 519 and 923 to 1224, dataset from which previous hydration results were derived [4,5,6]. We notice that for orbits 520 to 922 the calibration state is approximately half the nominal one and is stable. For orbits 1225 to 1650 the calibration state reaches six different approximate stable levels. The physical origin of these variations is still unknown and does not seem to be correlated with the variations of other instrumental parameters.

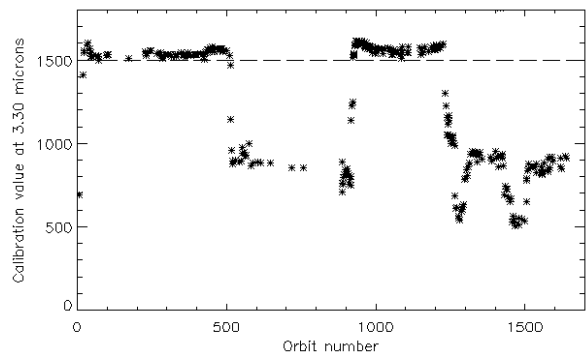


Figure 1 : Evolution of OMEGA L channel response to calibration lamp (value at 3.3  $\mu\text{m}$ ) with the orbit number. Values close to 1500 are considered as nominal.

The variations in calibration state have strong consequences for the derivation of albedo spectra. Fig. 2 shows two observations of a same area acquired very close in time, at  $L_s = 47^\circ$  (orbit 511) and  $L_s = 51^\circ$  (orbit 544). Between these two observations a strong varia-

tion of the L channel response to calibration lamp occurs (Fig. 2a). These two observations are supposed to give the same albedo spectra, and it is the case for the C channel (Fig. 2b). For the L channel, we can see that if both observations are processed with the same transfer function, the albedo spectrum of orbit 544 is strictly lower than that of orbit 511. The L channel albedo spectrum of orbit 544 is therefore wrong and requires an adapted transfer function for this calibration level. We also notice that albedo variation is not linearly linked to the calibration lamp variation. The response to calibration lamp is therefore an indication of the calibration state but cannot be used to derive a transfer function for this level.

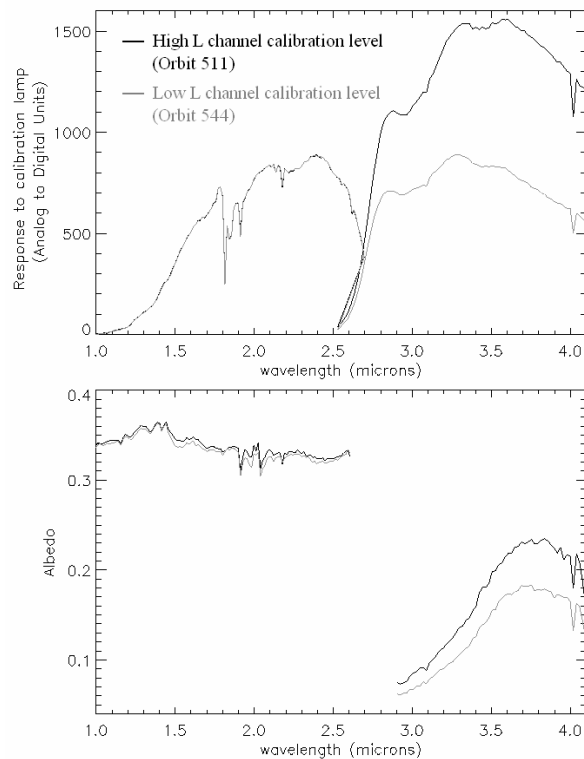


Figure 2: Example of the influence of instrumental variations on reflectance spectra. (a): OMEGA responses to calibration lamp (C and L channels) for orbits 511 (black, high level) and 544 (gray, low level). (b): Two albedo spectra of the geographical point (321.5E, 5N), tracked twice at close times but with different calibration responses. Black: pixel from orbit 511 (high level); gray: pixel from orbit 544 (low level).

*Derivation of new transfer functions.* As shown in Fig. 1 the response to calibration lamp presents several stability levels during which the transfer function must be constant. We therefore aim at determining a transfer function for each of these stages.

The method we use is based on the comparison of OMEGA overlapping observations acquired close in

time before and after a calibration transition. Fig. 3 illustrates such an overlapping for orbits 511 (reference observation) and 544 (observation to recalibrate). For each pixel of orbit 511 in the common area, a pixel of orbit 544 observes the same point of the surface. Because the two observations are close in time we suppose no change in surface composition occurred, therefore albedo spectra are supposed to be the same. The difference we obtain between the two observations is assumed to be caused by the variation of the instrument.

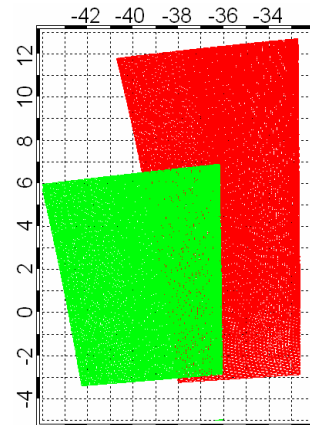


Figure 3 : Projection of an extract of orbits 511 (red) and 544 (green). The calibration measures of these two orbits are strongly different. The comparison of spectra on the overlapping area is used to derive a new transfer function.

The method consists in constructing the radiance spectrum of a pixel in orbit 544 from the corresponding pixel in orbit 511 (solar light diffusion plus thermal emission), and to derive the difference between this constructed spectrum and the acquired one. The albedo spectrum of a point in orbit 511 is first multiplied by the solar spectrum assuming lambertian diffusion. Then this spectrum is added to a predicted thermal emission of orbit 544. To get this thermal emission, the a priori surface temperature for orbit 544 is calculated from the surface temperature of orbit 511 and from the difference in solar insulation conditions. The constructed radiance spectrum for orbit 544 is the addition of these two components. The ratio between this spectrum and the radiance spectrum actually acquired is assumed to be the ratio between the nominal transfer function and the transfer function of orbit 544. By this way this couple of pixels provides a new temporary transfer function for the orbit to recalibrate.

This method is applied for each pixel of the couple of orbits 511 / 544. Pixels presenting water ice features (presence of a 1.5  $\mu\text{m}$  absorption band) are excluded from the averaging, as well as pixels presenting impor-

tant difference in continuum level or slope between the two observations (assumed to be due to atmospheric variations) or pixels presenting too strong difference in solar incidence (the amounts of aerosols in the light path is different). An averaged transfer function is then derived for this couple of orbits.

For the transition of the calibration state at orbit 520 in Fig. 1, every overlapping couple of orbits just before and after the transition is listed. A transfer function is derived for each couple, and the mean transfer function of all couples is taken as the new transfer function for orbits 520 to 922. The new transfer function is presented on Fig. 4, and its application on an OMEGA example spectrum is presented on Fig. 5.

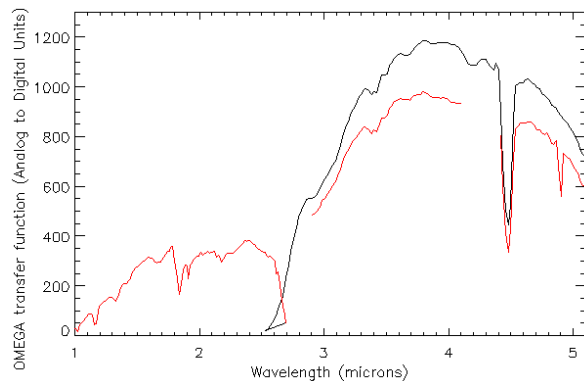


Figure 4 : OMEGA nominal transfer function (black) and new transfer function for orbits 520 to 922 (red). The value of the new transfer function is not to consider from 4.1  $\mu\text{m}$  to 4.4  $\mu\text{m}$  because of atmospheric absorptions of the signal from the surface.

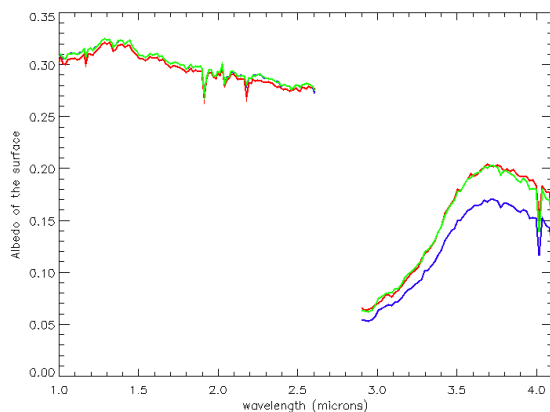


Figure 5 : Application of the new transfer function of orbits 520 to 920. Red curve: reference albedo spectrum extracted from orbit 511. Blue curve: albedo spectrum of the corresponding pixel in orbit 544, processed with the nominal transfer function. Green curve: albedo spectrum of the corresponding pixel in orbit 544, processed with the new transfer function.

The same work has now to be done for orbits 1225 to 1650. Six new transfer functions can be derived for these orbits, corresponding to the six successive identified steps. Fig. 6 shows the spatial positions of the different groups of orbits on Mars: orbits 1225 to 1650 cover large areas in the southern hemisphere, where few data about hydration have been studied so far.

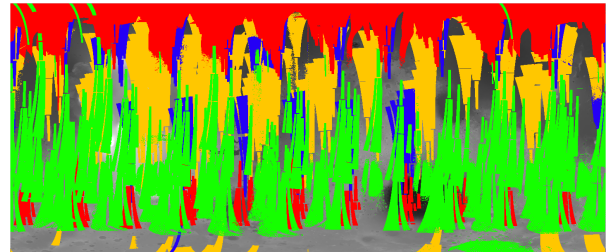


Figure 6 : Map on a Martian planisphere of the position of OMEGA data according to their calibration level. Red corresponds to orbits 40 to 519 (nominal level), blue to orbits 520 to 922, yellow to orbits 923 to 1224 (nominal level) and green to orbits 1225 to 1650.

**Refined water ice detection:** Water ice creates a strong absorption band from 3.0 to 3.4  $\mu\text{m}$  that makes the hydration measure at 3.0  $\mu\text{m}$  erroneous. In the previous hydration studies [4,5], every pixel exhibiting water ice features has therefore to be removed from the global study. This exclusion is based on the depth of the 1.5  $\mu\text{m}$  water ice absorption band which is rejected if greater than 1%. However instrumental non-linearities affects this band: its value may change by a few percent with the received light flux. The choice of the 1% value means that a lot of non icy pixel are ignored but no icy pixels are included. We propose here a method to correct the non-linearity problem so as to process much more non icy pixels.

Fig. 7 presents the value of the 1.5  $\mu\text{m}$  band depth versus the received light flux for a OMEGA orbit containing no water ice. We can see that the instrumental linearity defect makes the value vary from 1.02 to 0.99 whereas this value should be close to 0. The variations are approximately the same for all OMEGA orbits, in particular with a minimum around 1100 DN and a maximum around 1400DN, with possible slight shifts. A mean curve, in red, was derived from all OMEGA non icy data, and each band depth value is divided by this curve at its DN level to correct the linearity effect. The possible shift between the curve and the distribution shape is taken into account. The black distribution is then transformed to the green one which is much closer to 0. With this correction, all points exceeding a band depth value of 0.6% are then excluded from the global study. Such a threshold removes icy pixels more accurately and keeps more non icy ones.

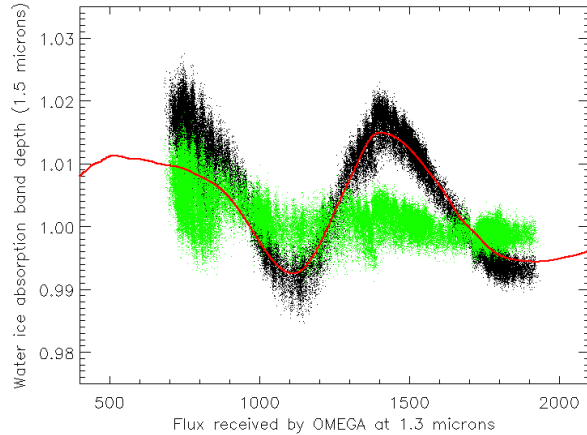


Figure 7 : Linearity problem of the water ice band with the received light flux. Black: for all pixels of a given data cube (without ice), value of the 1.5  $\mu\text{m}$  water ice band depth versus the received flux (in ADU). This value may vary by a few percent due to instrumental defects. Red: average linearity curve of the OMEGA instrument. Green: new value of water ice band depth after correction by the linearity curve.

**First results:** Previous studies about hydration from OMEGA data [4,5,6] represented  $\sim 30\%$  of the Martian surface. Thanks to the recalibration of the non-nominal L channel data and to the better water ice diagnostic, we will be able to access to the hydration of more than 60% of the Martian surface. In particular we

should improve our knowledge of the southern hemisphere.

Important results about the hydration of the Martian surface were presented by previous studies [4,5,6]: the 3  $\mu\text{m}$  band is present everywhere on Mars, its strength increases with albedo, decreases slightly with altimetry, the 3  $\mu\text{m}$  band is enhanced in places where phyllosilicates or sulfates have been diagnosed, it is also enhanced in the latitudes greater than  $60^\circ\text{N}$ . Moreover temporal variations of hydration were detected in the northern mid-latitudes.

An new hydration map is presented on Fig. 8 including the whole OMEGA dataset from orbit 40 to 1224. In particular the data from orbits 520 to 922 are processed with the new transfer function, but data from orbits 1225 to 1650 are not present. On this map, the new hydration data (corresponding to blue data on Fig 6) overlap well with the former ones. The hydration results related to these data are consistent with the former studies [4,5,6] and reveal the same trends.

**References:** [1] Bibring, J. P., et al. (2004), *letters to nature*, 428, 627-630. [2] Titov, D. V. (2002), *Adv. Space Res*, 29, 183-191. [3] Feldman, W. C., et al. (2004), *JGR*, 109, CiteID E09006. [4] Jouglet D. et al. (2006) *LPS XXXVII*, Abstract #1741. [5] Jouglet D. et al. (2007) *JGR*, in press. [6] Milliken R. E. et al. (2007) *JGR*, in press. [7] Yen A.S. et al. (1998) *JGR*, 103, 11,125-11,133.

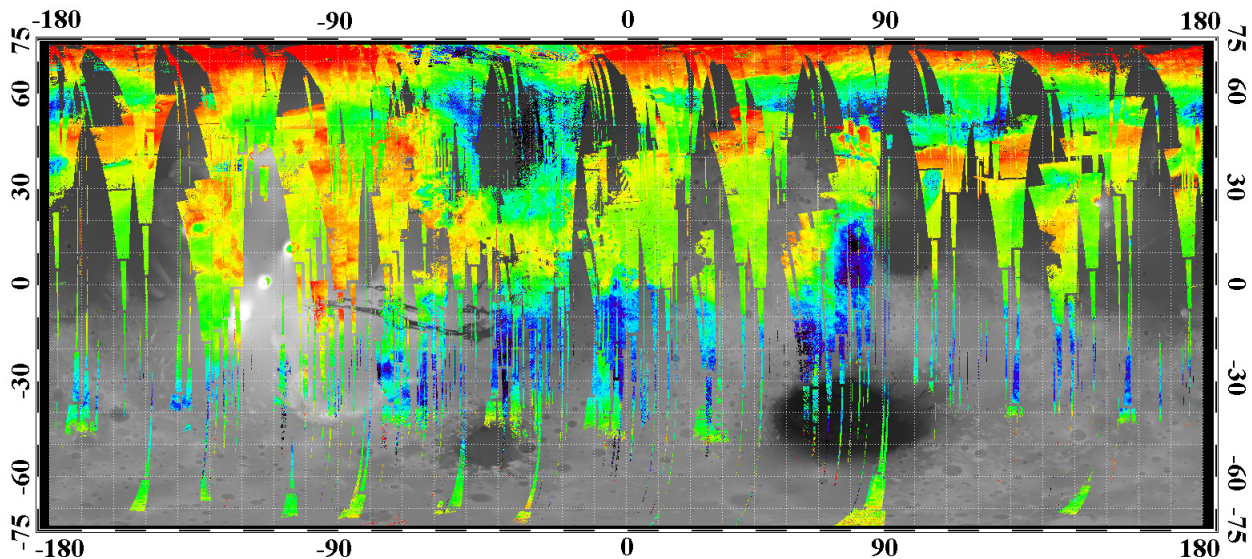


Figure 8 : Map over the MOLA altimetry of the 3  $\mu\text{m}$  hydration feature estimated by the integrated band depth. The dataset corresponds to orbits 40 to 1224 with adapted transfer functions. 0.25  0.52